

Retinal ganglion cell synchronization by fixational eye movements improves feature estimation

Martin Greschner¹, Markus Bongard¹, Pal Rujan² and Josef Ammermüller¹

¹ Department of Biology, Neurobiology Group, University of Oldenburg and ² Department of Physics, Complex Systems Group, University of Oldenburg, 26111-Oldenburg, Germany

Correspondence should be addressed to J.A. (josef.ammermueller@uni-oldenburg.de)

Published online: 4 March 2002, DOI: 10.1038/nn821

Image movements relative to the retina are essential for the visual perception of stationary objects during fixation. Here we have measured fixational eye and head movements of the turtle, and determined their effects on the activity of retinal ganglion cells by simulating the movements on the isolated retina. We show that ganglion cells respond mainly to components of periodic eye movement that have amplitudes of roughly the diameter of a photoreceptor. Drift or small head movements have little effect. Driven cells that are located along contrast borders are synchronized, which reliably signals a preceding movement. In an artificial neural network, the estimation of spatial frequencies for various square wave gratings improves when timelocked to this synchronization. This could potentially improve stimulus feature estimation by the brain.

Recognition of visual stimulus features depends on the flow of action potentials from retinal ganglion cells to the brain. The basic features of time-varying stimuli can be estimated from the activity of the ganglion cell population by using artificial neural networks, discriminant analysis or linear decoders^{1–6}. For a completely stationary stimulus, the activity in the visual system is largely reduced, however, because this system responds mainly to changes^{7,8}. This is consistent with the observation that visual perception fades away when the image of an object is stabilized artificially on the retina^{9,10}. Therefore, during normal fixation in a stationary visual world, relative image movements that turn any stationary visual scene into a spatiotemporal varying image on the retina are necessary to maintain perception^{11,12}.

Reconstructing time-varying stimuli with linear decoders or artificial neural networks saturates as spike trains from 8 to 14 retinal ganglion cells are recruited^{1,6}. Reconstruction at this point is still lacking much of the true stimulus, probably as a consequence of the phototransduction process and broadband noise in the retinal circuitry^{1,4}. By contrast, stimulus estimation using discriminant analysis or neural networks is nearly perfect when an external reference signal temporally locks the estimation procedure to the time intervals following each stimulus change^{2,3,5}. With this timelocked procedure, latency differences and the initial spike rate are included into each single estimation. Latency and rate are proposed to be the most important encoding mechanisms for, for example, changes in the magnitude of contrast^{3,13,14}.

Eye and head movements during fixation of a stationary stimulus induce spatiotemporal image changes on the retina. Fixational eye movements influence the firing probability of single cortical cells, and it has been speculated that this could produce synchronous activity^{15–19}. If synchronization reliably encodes stimulus changes, then it could be used to determine latency and initial rate.

We have therefore examined the relationship between fixational eye movements and the activity of retinal ganglion cells in the turtle. We determined whether such movements synchronize ganglion cell activity, and whether feature estimation is better when it is timelocked to stimulus changes rather than when it is not. We show that fixational eye movements do exist in the turtle, and that they drive and synchronize retinal ganglion cells. Feature estimation is improved when timelocked to this synchronization, which is driven by the stimulus changes induced by eye movement.

RESULTS

Turtles show miniature eye movements during fixation

We measured eye and head movements of the resting turtle (*Pseudemys scripta elegans*) using video-oculography. Because our study was focused on image motion on the retina of a stationary stimulus during fixation, we did not analyze large-amplitude movements such as saccades and head turns, which completely change the direction of gaze.

During these 'stable' periods of gaze, residual head movements ($11.77 \pm 8.59 \mu\text{m/s}$ velocity on the retina; $n = 80$) still contributed to the total image movement (Fig. 1a, inset). After subtracting head movements, a small and slow drift-like eye movement component ($6.7 \pm 2.9 \mu\text{m/s}$) persisted, which was superimposed by larger and faster periodic components. Fast Fourier transform (FFT) analysis identified a broad peak in the spectrum of amplitude density at about 5 Hz for the periodic component (Fig. 1a). Its x and y amplitude distribution peaked at about $5 \mu\text{m}$ on the retina, which yielded oblique movements of about $7 \mu\text{m}$ (Fig. 1b). The velocity (v) of forward and backward movement increased roughly linearly with amplitude (a) and was described by $v (\mu\text{m/s}) = 256 \pm 20 (\text{s}^{-1}) \times a (\mu\text{m})$; adjusted R square (R^2) = 0.48.



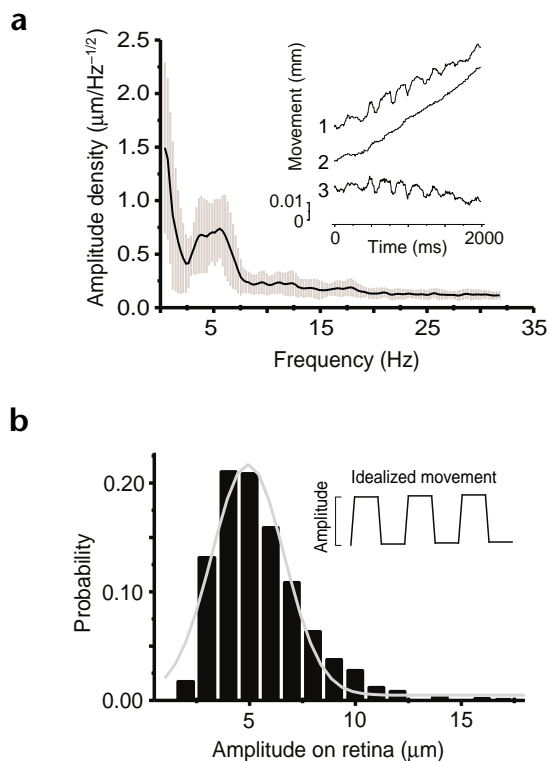


Fig. 1. Eye movements of the turtle during fixation. **(a)** Mean amplitude density spectrum of the components of eye movement. Two-second time intervals such as those in trace 3 of the inset were analyzed by FFT and averaged. Data are collapsed from horizontal and vertical movement. The first peak correlates to the drift-like eye movement and the second peak at around 5 Hz correlates to the periodic component (shaded area represents s.d.; $n = 80$). Inset shows the original video-oculographic recording of total pupil movement (1), head movement (2) and pure eye movement (3 = 1 - 2). Only horizontal movement is shown. Scale bar indicates movement amplitude in the focal plane of the EyeLink camera. **(b)** Peak amplitude distribution of the periodic component ($n = 1,500$). Inset shows the idealized stimulation scheme used for simulating periodic movement. The rising (and falling) time of movement steps was 5 ms, with speed adjusted linearly to amplitude as found in natural movements.

Thus, turtle eyes move periodically during fixation with retinal amplitudes on the order of the diameter of a photoreceptor²⁰. Because there are clear interspecies differences in eye movements, we do not use terminology derived from other species but use the general terms ‘drift-like’ and ‘periodic’ to describe the two fixational eye movements.

Fixational eye movements increase retinal activity

Instead of moving the fixating eye, an image was moved on an isolated retina and the effects of this simulated fixational movement on ganglion cell activity were measured. Single- and multi-unit activities were recorded by using a square 10×10 multi-electrode array. After a control period in darkness (Fig. 2a, ‘dark’), a stationary square wave grating—the contrast borders of which were aligned with the electrode rows—was projected onto the retina (Fig. 2a, ‘light on’). This elicited an initial, transient population response that adapted within a few seconds to a steady-state value below that observed in darkness (Fig. 2b). This reduction in activity to prolonged illumination with the stationary grating was seen in most units, even in those that were initially excited by light on (Fig. 2a, arrows).

Fig. 2. Periodic eye movements increase retinal activity. **(a)** Continuous recording from 54 units during darkness, after switching on a stationary square wave grating and during wobbling of this grating. The grating was wobbled using the time course of the original periodic eye movement data shown in Fig. 1. At the end, wobbling was stopped for control measurements. Arrows indicate examples of units that were initially excited by light on, but were later inhibited during prolonged illumination with the stationary grating. The grating spatial period was 1.35 cycles/mm (each row of electrodes of the multi-electrode array was aligned with a contrast border). **(b)** Total population and mean single-unit activity from data shown in (a); bin width, 1 s. Horizontal lines show average activity for the steady state under each condition.

Spatial displacements were introduced that mimicked the spatial and temporal characteristics of the video-oculographic measurements obtained in the intact animal, which simulated the image flow on the retina induced by actual turtle eye movements (Fig. 2a, ‘wobbling’). This immediately increased the activity of both the population and single units. The following control with a stationary grating confirmed that the recording conditions had not changed.

Mean single-unit activities during the dark, stationary and wobbling conditions were 0.89 ± 0.16 , 0.31 ± 0.18 and 0.71 ± 0.17 spikes/unit \times s, respectively. The mean values during darkness corresponded to those from a previous study²¹. The steady-state stationary and wobbling values were significantly different (Fig. 2b; measured in 40-s intervals during steady state with 1-s time bins; t -test, $p < 0.0001$). The mean values from eight retinas were 0.43 ± 0.49 and 0.79 ± 0.93 spikes/unit \times s, respectively ($n = 246$ units). Activities varied considerably because different proportions of the various ganglion cell types were recorded in different retinas. In a given experiment, activity was always significantly higher during the wobbling than during the stationary condition.

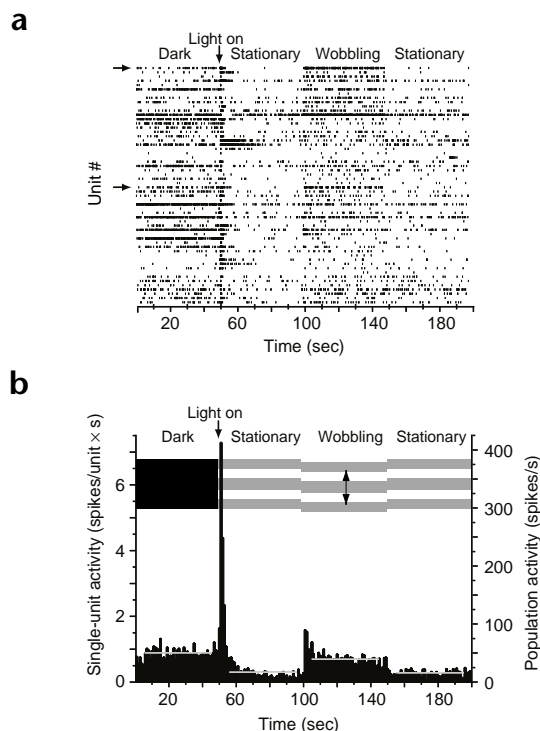
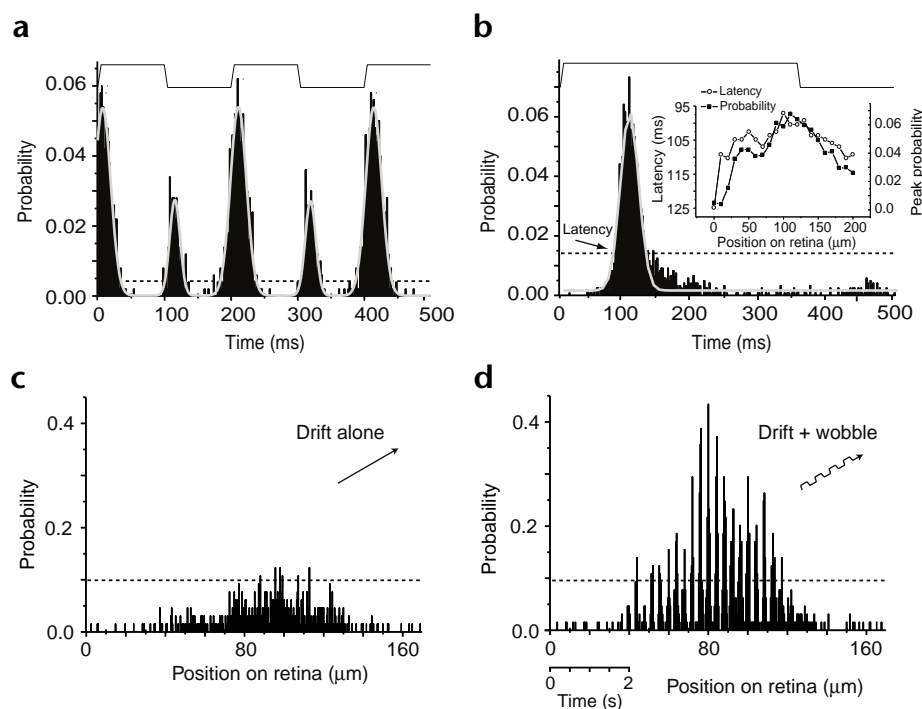


Fig. 3. Single-unit responses to fixational eye movements. **(a)** PSTH of a single unit in response to a contrast border wobbling under an idealized movement scheme (top trace). This unit responded with different probabilities to forward and backward movement. Stimulation, 5 Hz; duty cycle, 0.5; amplitude, 5 μm ; grating frequency, 1.35 cycles/mm; bin width, 2 ms; 500 repetitions. A probability of 1 corresponds to 1 spike/bin (500 Hz) for one repetition. Dashed line indicates 99% confidence limit in this and the following figures. Gray curves indicate Gaussian fits of the data. **(b)** Lower frequency wobbling of another unit (stimulation, 2 Hz; duty cycle, 0.7; amplitude, 5 μm ; 600 repetitions). Latency (arrow indicates the crossing point of Gaussian fit with confidence limit) varied around 100 ms. Inset shows that displacement of the wobbling contrast border in 10- μm steps yielded receptive field-like optimum curves for peak response probabilities and latencies. Latencies are plotted with decreasing values upwards. **(c)** Responses of a single unit to a drifting contrast border (velocity, 20 $\mu\text{m}/\text{s}$; bin width, 20 ms; 65 repetitions). **(d)** Response of the same unit to the same drift, superimposed with periodic 5-Hz, 5- μm amplitude wobbling (bin width, 20 ms; 65 repetitions).



These results show that transforming an originally stationary image into one that varies spatiotemporally—thus mimicking real fixational eye movements—enhances retinal activity.

Single-unit response profiles to fixational movements

For the analysis of single-unit activity, we used idealized step-like movement schemes within the range of the movement data because we could control the independent variables better. The occurrence of a spike in single units was correlated significantly with movement steps (Fig. 3a). In some units, significant responses were reached with amplitudes as small as 3 μm on the retina. For amplitudes between 5 and 9 μm , the relative peak response probability (p) increased roughly linearly with the amplitude (a) of the movement step ($p = 0.21a$; $R^2 = 0.97$, $n = 12$). Stimulation with wobbling frequencies at about 5 Hz led to the initially unexpected result that responses had very short latencies (Fig. 3a). Analysis with 2-Hz stimulation showed that the average latencies were 107 ± 26 ms ($n = 100$ units; Fig. 3b). Therefore, this phase lag aligned responses to forward movements with the following backward movement, and vice versa, for wobbling at 5 Hz.

Latencies and peak response probabilities depended on the position of the contrast border within the receptive fields of the cells (Fig. 3b, inset). Peak response probabilities and latencies followed optimum curves, with the maximum peak probability close to the position where minimum latency was measured. Optimal positions were often displaced from the electrode positions because the receptive fields were generally not centered around the electrodes. Different units responded differentially to forward and backward movements. Some units responded to movement in both directions either with the same probability or with different probabilities, whereas other units responded only in one direction (Fig. 3a and b).

So far, the possible effects of the small head or drift-like eye movements, as seen in the oculographic measurements, had been neglected. To study these effects, responses to gratings that drifted with constant velocity were compared with responses to gratings with the same mean drift but with superimposed periodic components (Fig. 3c and d). The threshold for a significant response to drift alone was around 20 $\mu\text{m}/\text{s}$ for the best units that we recorded (Fig. 3c). This is near the upper limit of the measured values for drift and head movements in the intact animal during fixation. Therefore, under these viewing conditions slow movements do not seem to have a principal role. Superposition of drift with periodic movement showed that there were significant responses to the periodic components (Fig. 3d). As above, peak response probabilities followed the profiles of the receptive fields. Although higher drift speeds (tested up to 1.6 mm/s) produced significant responses to drift alone, the periodic responses to superimposed periodic movement were conserved or even enhanced (data not shown).

This shows that ganglion cells located along a contrast border are driven mainly by the periodic eye movement components, even in the presence of drift. For each cell there exists an optimal position of the contrast border, at which the responses show highest probability and shortest latency.

Synchronization reliably encodes movement steps

We studied how reliable stimulus movement can be detected from the activity from single and multiple units. We defined synchronization as near-coincidence firing between units if correlated spikes were centered around zero in the cross-correlograms²².

Simulated periodic movements synchronized units that were aligned with contrast borders. On average, $25.7 \pm 23.2\%$ ($n = 120$) of the cells were synchronized by a wobbling grating (Fig. 4a).

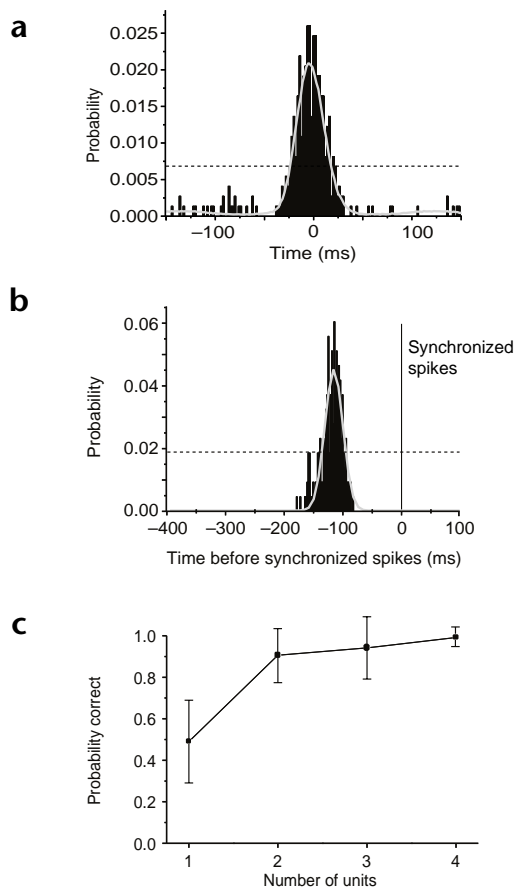


Fig. 4. Synchronization signals a preceding movement. **(a)** Cross-correlogram of two units aligned with a contrast border. Gray curve indicates the envelope of the shuffled cross-correlogram (the 'shift predictor'). The difference between the raw correlation and the shift predictor stayed below confidence limit (bin width, 2 ms; 729 repetitions). **(b)** Temporal precision and probability that a movement step preceded synchronized spikes for one cell pair. Wobbling frequency was set at 2 Hz to measure the real delay, which was unaffected by the lag phase of the cells (grating frequency, 1.35 cycles/mm; bin width, 2 ms; 600 repetitions). Gray curve shows the Gaussian fit of the data. **(c)** Dependence of correctly coded movement steps on the number of synchronized units compared with the performance of single units ($n = 12$ in each case).

Synchronization was rather broad, with a mean width of the Gaussian fit of 31.9 ± 6.5 ms ($n = 60$ synchronized pairs). Shuffling of the cross-correlograms (the 'shift predictor'; Fig. 4a, gray line) led to distributions that were very similar to the raw correlograms. Synchronization was absent or below confidence levels in the corrected correlograms, after subtracting the shift predictor from the raw data ($n = 60$). This strongly indicated that synchronization was caused by covariation in firing rate, which was driven by the simulated eye movements, and was not the result of internal connectivity or common input. This was supported by the fact that no synchronization could be detected with a completely stationary grating or in darkness (tested with the same cell pairs). Synchronization did not depend on distance of the synchronized units (measured in the range 0.4–4 mm).

We took the position of the brain, which 'sees' only incoming spike trains, and determined the probability that a synchronized activity is preceded by a movement step (reverse correlation). First we determined synchronized units, using the measured 32-ms mean synchronization width identified above as an additional criterion. This was done for pairs, triples and quadruples of cells. From these synchronized pairs (or triples or quadruples), we then selected those spikes that occurred within 32 ms of each other from the total spike trains. These synchronized spikes (such as those in Fig. 4a) were taken as reference time points ($t_0 = 0$) and cross-correlation was done with the preceding movement steps (Fig. 4b). Each reverse correlation was fitted with a Gaussian, using width and crossing of significance level as measures for temporal precision and time delay, respectively. The mean time delay, which indicates the time that movement

occurred before the synchronized spikes, was -91 ± 3 ms ($n = 60$). The mean width for the reverse correlation was 33 ± 1 ms ($n = 60$). As expected, measured synchronization between multiple units was rare, because the fraction ($n_{\text{sync}}/n_{\text{total}}$) of synchronized spikes (n_{sync}) in the total spike number (n_{total}) of the respective synchronized units decreased from 0.288 (pairs) to 0.090 (triples) to 0.016 (quadruples).

We calculated the reliability for coding the preceding movement. First, the crossing points of the Gaussian fit with significance level were determined (Fig. 4b). Second, the probabilities from the time bins between these points were summed up. This value was related to the sum of probabilities from all time bins, which yielded a relative value of 'probability correct'. It indicates the percentage of synchronized spikes that encode preceding movement within the time window determined by the significant part of the reverse correlations.

We then compared the results from synchronized units with those obtained from single units (Fig. 4c). The mean 'probability correct' for spikes from single units was 0.5. This value increased steeply to 0.9 with two synchronized units, and reached unity when the synchronized spikes of four units were examined. To test whether the high values of probability correct for synchronized units were caused by internal connectivity, we shuffled the trials. We found no statistical difference between shuffled and unshuffled groups; therefore, the results are due to stimulus-driven synchronization. Thus, if the brain had to decide whether a stimulus movement step preceded a spike from a single unit, it would be wrong in 50% of the cases; however, it would be close to perfect if synchronized spikes arrived.

Synchronization improves feature estimation

Does this additional information have any potential value for feature estimation? To examine this, we stimulated the retina with four contrast gratings with different spatial frequencies. An artificial neural network ('perceptron') was used as a classifier that estimated the original grating frequency from the patterns of ganglion cell activity. Conditions in which information about the occurrence of movement steps was used were compared with conditions in which this information was not used.

From the recordings, 256-ms intervals were selected and transformed to bitmaps, which represented the activity pattern of the recorded ensembles (Fig. 5a; see Methods and Supplementary Methods). The perceptron then estimated grating spatial frequency from single examples of these bitmaps. We tested two conditions in which estimation was timelocked to movement steps. Either each bitmap was obtained by locking the 256-ms time interval to the synchronized spikes of a synchronized cell pair ($t = 0$; Fig. 5a), or the corresponding bitmap from the identical movement period was obtained by locking the time interval to the external trigger signal from the stim-



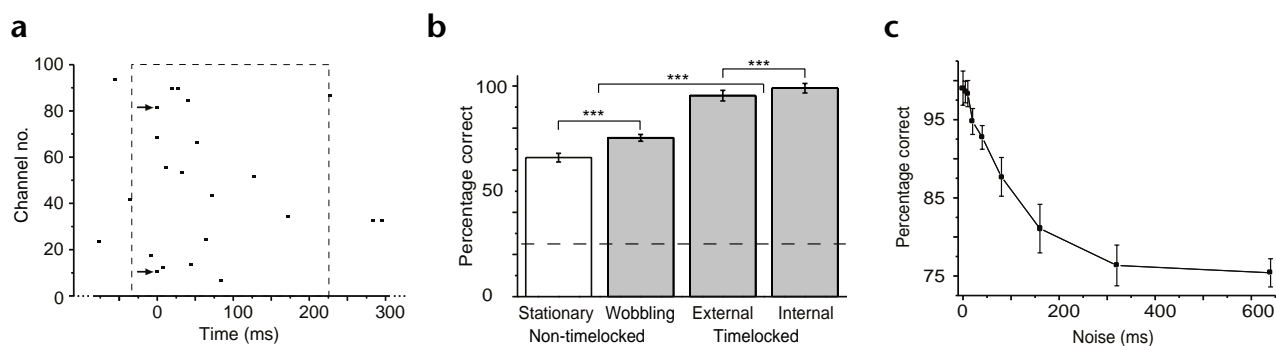


Fig. 5. Grating frequency estimation improves when timelocked to synchronization. Four different gratings (0.68, 1.35, 2.70 and 5.41 cycles/mm; wobbling frequency, 2 Hz; amplitude, 7 μm) were used for stimulation. Grating frequency was estimated by a perceptron from the recorded population activity. **(a)** Example of a 256-ms interval, cut from a continuous recording, that contains the activity pattern of all recorded cells. The interval was timelocked to synchronized activity (arrows) from the chosen cell pair ($t_0 = 0$). **(b)** Percentage of correct estimation for timelocked and non-timelocked conditions. Dashed line indicates the 25% chance rate. **(c)** Dependence of correct estimation on external noise added to synchronization. Random temporal jitter with different maximal amplitudes was added to each t_0 . Fifteen cell pairs were analyzed in **(b)** and **(c)**.

ulus computer. For the non-timelocked condition, the time intervals were chosen randomly in the same movement periods as above. Thus, identical movement periods were compared in these three conditions, and only the starting points of the bitmaps differed. As a control, grating frequency was estimated with randomly chosen time intervals from experiments using stationary gratings.

As expected, estimation was good when timelocked to the external trigger signal (Fig. 5b; $95.4 \pm 2.5\%$ correct; $n = 15$ synchronized pairs). This agrees with earlier feature estimation studies that used discriminant analysis or neural network analysis, together with an external reference signal^{2,3,5}. Estimation with bitmaps timelocked to synchronized activity yielded significantly better results ($99.0 \pm 2.2\%$ correct; $n = 15$; $p = 0.0002$; unpaired t -test). Estimations with randomly chosen bitmaps from wobbling grating experiments and from stationary grating experiments, by contrast, were significantly worse ($75.4 \pm 1.5\%$ and $66.0 \pm 2.0\%$ correct, respectively; $n = 15$; t -test; $p < 0.0001$ in both cases) when compared with the timelocked conditions. The difference between the latter two conditions was also significant ($p < 0.0001$).

To measure the precision that is needed to estimate grating spatial frequency correctly under conditions in which bitmaps were locked to internal synchronization, we added external temporal noise to each synchronization signal (Fig. 5a, t_0). Increasing external noise degraded performance rapidly (Fig. 5c). The drop was steep for low amplitudes of noise, and noise in excess of about 200 ms resulted in values that were indistinguishable from those obtained with random start signals.

These results show that grating frequency estimation that is timelocked to internal synchronization is superior to estimation that is non-timelocked.

DISCUSSION

Retinal image movement during fixation was composed of three components: periodic movements were superimposed on small eye drift and slow head movements. Given that peak amplitudes varied around the diameter of a photoreceptor, the periodic component could tentatively be compared with tremor in humans²³. The frequency was about 5 Hz, however, compared with 70–100 Hz in humans²⁴. This difference in frequency might be because the turtle is a cold-blooded animal and the tonic firing of oculomotor neurons is probably reduced²⁵.

The drift components, which were present during stable periods of gaze, did not evoke significant responses and, more notably, did not degrade the responses to the periodic components. The responses to these periodic movements support the idea that hyperacuity is a general property of the receptive fields of ganglion cells²⁶. These cells respond to displacements that are more than one order of magnitude smaller than the radius of their receptive field centers. Synchronization driven by these periodic components reliably encoded the occurrence of movement steps and was therefore an excellent signal to timelock activity bitmaps with stimulus changes for feature estimation.

Neural networks have been shown to function exactly like a linear multineuronal decoder and were used here to estimate the spatial grating frequency¹. Estimation was best when the bitmaps were timelocked to movement steps. In such a condition, relative latency and initial spike rate will be contained in each bitmap. These parameters are the most important variables for discriminating, for example, contrast⁵. In the turtle, retinal ganglion cells latencies to light flashes are 100–300 ms (short latencies) or above 400 ms (long latencies)²⁷. The latencies of optimally located synchronized units (90–100 ms) would be short enough to provide a signal for relative latency determination. In particular, direction-selective cells might be candidates for short-latency responses to periodic eye movements^{21,28}.

Estimation was better when timelocked to internal synchronization, as compared with the external trigger signal, although for an objective observer the external signal is more precise than the internal synchronization. This result can be explained if the temporal interdependencies between spikes, which arise from interactions within the retina, are preserved better than spike timings with respect to the external signal⁴. If this is the case, then the perceptron estimation will be better with internal synchronization as a starting signal, because the activity pattern of the bitmaps for the different movement steps will be more similar for a given grating frequency. This will increase the number of correct estimations.

By contrast, adding external jitter to the internal synchronization rapidly degraded feature estimation, as expected. Therefore, temporal precision seems to be important with respect to internal synchronization, but not necessarily with respect to the external signal. This does not exclude higher precision of synchronization with respect to the external trigger signals²⁹, which we could not



measure owing to technical limitations (see Supplementary Methods). This would probably increase further the correct estimation with synchronization as starting point. Grating frequency estimation with randomly starting bitmaps was well above the chance rate because some relevant information would still be included in the bitmaps. For example, the mean activity of the population depended on grating spatial frequency—both for stationary and wobbling conditions—and showed an optimum at 1.35 cycles/mm (data not shown).

The dependence of spike probability and latency from contrast border position implies that both movement onset and the spatial properties of a stationary visual scene are signaled to the brain. A good strategy for detecting eye movements would involve examining synchronous activity from large populations of cells—if eye movements are to be discerned from object movements. For any given fixational movement, all optimally placed ganglion cells will respond fastest and with highest probability, and many will be synchronized with each other. The first strong, synchronized activity will thus arise from the ensemble of cells that represents the spatial structure of the scene, and this activity will signal that a stimulus change has occurred. Later incoming activity can then be used for further feature detection³⁰.

Estimation of simple visual features such as color or intensity saturates with unexpectedly low numbers of cells^{1–3,5}. Natural scenes from short periods of movies can be reconstructed with as few as 6–8 pairs of cells for each point in space³¹. There is no reason why this should not be possible for stationary objects, which are transformed actively to a temporally changing retinal image by eye, head and body movements.

METHODS

Eye movement measurements. We measured miniature eye movements in three turtles (*Pseudemys scripta elegans*) using infrared video-oculography (Eyelink, SensoMotoric Instruments, Berlin, Germany). The apparatus was adapted for use with turtles. Two cameras measured pupil and head movements simultaneously (see Supplementary Methods). The setup was calibrated with an artificial pupil and head in the focal planes. We obtained different conversion factors for head and eye movements after applying a schematic turtle eye³² (83.7 μ m on the retina per degree of visual angle for eye movements; 0.44 mm on the retina per mm of displacement on the focal plane of the camera for head movements). We analyzed data by PowerLab software (AD Instruments, Hastings, UK) using the FFT, amplitude histogram and differentiate extensions.

Electrophysiological recording. Electrophysiological experiments were done on 20 isolated retinas from 12 turtles. Animals were killed according to the University of Oldenburg Ethical Committee and to ECC rules (86/609/ECC). We isolated retinas and made recordings as described, using the acute Utah 100-electrode array (Bionic Technologies, Salt Lake City, Utah)^{3–5,33}. The retinas were stimulated via an optical bench with a Xenon light source (150 W), neutral density filters, shutter and aperture. Square wave gratings (0.68, 1.35, 2.70 and 5.41 cycles/mm on the retina; 40 lx and 2.6 lx retinal illuminance through the bright and dark stripes, respectively) were projected onto the retina through an x - y miniature mirror system (Datronic, Rastede, Germany). We moved the mirrors using a separate stimulus computer, which was synchronized with the data acquisition computer.

Data processing and analysis. Typically several spike waveforms occurred at one electrode. An optimized Kohonen network separated these spike 'prototypes' (see Supplementary Methods). In general, multiprototype signals were obtained from 20 to 60 electrodes. We selected those electrodes that had waveforms typical of single-unit activity, which were unequivocal in terms of both amplitude and shape (typically from 10 to 60 prototypes). Data were stored as a sequence of 'time-stamped' events for each unit, and these events were used for further analysis. Peri-stimulus-time histograms (PSTH), cross-correlations, shift predictors and 99% confidence limits

were calculated with NEX Neuroexplorer (Nex Technologies, Lexington, Massachusetts). The 99% confidence limits were calculated assuming that spike trains are Poisson trains with mean frequencies. Gaussian fits were done with Mathematica (Wolfram Research, Champaign, Illinois). We used SPSS (SPSS, Chicago, Illinois) for statistical analysis. Quantitative values are reported as the mean \pm s.d.

Feature estimation. A perceptron with maximal stability was used to estimate grating spatial frequencies on the basis of the recorded activity of the ganglion cells (see Supplementary Methods)^{34,35}. Time intervals of 256 ms were selected from the data trains, which contained the activity of all measured units. Each interval contained a 30-ms period before its locking point, $t_0 = 0$, and a 226-ms period after t_0 . The preceding 30-ms period was introduced to take the average temporal width of spike synchronization (32 ms) into account. The 256-ms periods were transformed to activity bitmaps from which the spatial frequencies of four different square wave gratings had to be estimated. First, a cell pair was chosen whose spikes were synchronized by a given wobbling grating. Then all bitmaps, which were timelocked to the synchronized spike pairs, were constructed. Ninety were chosen randomly for estimation. This was done for each grating, which yielded a total of 360 bitmaps. The perceptron then estimated grating frequency from each of the 360 bitmaps. For each cell pair the percentage correct was calculated by (number of correctly assigned bitmaps/360) \times 100. This was compared with the estimation performance using bitmaps from the identical movement periods, timelocked to the external trigger signal, and bitmaps starting randomly within the same movement periods. We analyzed 15 synchronized cell pairs from four experiments in this way. As a control, randomly chosen bitmaps from experiments with stationary gratings were used for estimation. To exclude effects of neuron number, we used only experiments with more than 30 recorded units for this analysis (see Supplementary Methods).

Note: Supplementary Methods are available on the Nature Neuroscience web site

Acknowledgments

We thank S. Massey, R.A. Normann, R. Weiler and M. Greenlee for critically reading the manuscript. This work was supported by grants from the Deutsche Forschungsgemeinschaft and the European Community (CORTIVIS) to J.A.

Competing interests statement

The authors declare that they have no competing financial interests.

RECEIVED 13 NOVEMBER 2001; ACCEPTED 17 JANUARY 2002

1. Warland, D. K., Reinagel, P. & Meister, M. Decoding visual information from a population of retinal ganglion cells. *J. Neurophysiol.* **78**, 2336–2350 (1997).
2. Fernandez, J. M., Bolea, J. A., Ammermüller, J., Normann, R. A. & Fernandez, E. A neural network approach for the analysis of multineural recordings in retinal ganglion cells. *Lecture Notes Comp. Sci.* **1607**, 289–298 (1999).
3. Shoham, S. *et al.* The classification of spatial, chromatic, and intensity features of simple visual stimuli by a network of retinal ganglion cells. *Lecture Notes Comp. Sci.* **1240**, 44–53 (1997).
4. Normann, R. A., Warren, D., Ammermüller, J., Fernandez, E. & Guillery, S. High spatio-temporal mapping of visual pathways using multi-electrode arrays. *Vision Res.* **41**, 1261–1275 (2001).
5. Fernandez, E., Fernandez, J.-M., Ammermüller, J., & Normann, R. A. Population coding in spike trains of simultaneously recorded retinal ganglion cells. *Brain Res.* **887**, 222–229 (2000).
6. Meister, M. & Berry, M. J. II. The neural code of the retina. *Neuron* **22**, 435–450 (1999).
7. Hartline, H. K. The responses of single optic nerve fibers of the vertebrate eye to illumination of the retina. *Am. J. Physiol.* **121**, 400–415 (1938).
8. Hubel, D. & Wiesel, T. N. Receptive fields of single neurones in the cat's striate cortex. *J. Physiol. (Lond.)* **148**, 574–591 (1959).
9. Riggs, L. A. & Ratliff, F. The effects of counteracting the normal movements of the eye. *J. Opt. Soc. Am.* **42**, 872–873 (1952).
10. Ditchburn, R. W. & Ginsborg, B. L. Vision with a stabilized retinal image. *Nature* **170**, 36–37 (1952).
11. Barlow, H. B. Eye movements during fixation. *J. Physiol. (Lond.)* **116**, 290–306 (1952).

12. Steinman, R. M. & Levinson, J. Z. in *Eye Movements and Their Role in Visual and Cognitive Processes* (ed. Kowler, E.) 115–212 (Elsevier, Amsterdam, 1990).
13. Enroth-Cugell, C. & Shapley, R. M. Adaptation and dynamics of cat retinal ganglion cells. *J. Physiol. (Lond.)* 233, 271–309 (1973).
14. Kuffler, S. W. Discharge patterns and functional organization of mammalian retina. *J. Neurophysiol.* 16, 37–68 (1953).
15. Bair, W. & O'Keefe, L. P. The influence of fixational eye movements on the response of neurons in area MT of the macaque. *Vis. Neurosci.* 15, 779–786 (1998).
16. Leopold, D. A. & Logothetis, N. K. Microsaccades differentially modulate neural activity in the striate and extrastriate visual cortex. *Exp. Brain Res.* 123, 341–345 (1998).
17. Martinez-Conde, S., Machnik, S. L. & Hubel, D. H. Microsaccadic eye movements and firing of single cells in the striate cortex of macaque monkeys. *Nat. Neurosci.* 3, 251–258 (2000).
18. Gur, M., Beylin, A. & Snodderly, D. M. Response variability of neurons in primary visual cortex (V1) of alert monkeys. *J. Neurosci.* 17, 2914–2920 (1997).
19. Snodderly, D. M., Kagan, I. & Gur, M. Selective activation of visual cortex neurons by fixational eye movements: implications for neural coding. *Vis. Neurosci.* 18, 259–277 (2001).
20. Kolb, H. & Jones, J. The distinction by light and electron microscopy of two types of cone containing colorless oil droplets in the retina of the turtle. *Vision Res.* 27, 1445–1458 (1987).
21. Granda, A. M. & Fulbrook, J. E. Classification of turtle retinal ganglion cells. *J. Neurophysiol.* 62, 723–737 (1989).
22. Brivanlou, I. C. H., Warland, D. K. & Meister, M. Mechanisms of concerted firing among retinal ganglion cells. *Neuron* 20, 527–539 (1998).
23. Fahle, M. Psychophysical measurement of eye drifts and tremor by dichoptic or monocular vernier acuity. *Vision Res.* 31, 209–222 (1991).
24. Eizenman, M., Hallett, P. E. & Frecker, R. C. Power spectra for ocular drift and tremor. *Vision Res.* 25, 1635–1640 (1985).
25. Coakley, D. *Minute Eye Movement and Brain Stem Function* (CRC Press, Boca Raton, Florida, 1983).
26. Shapley, R. & Victor, J. Hyperacuity in cat retinal ganglion cells. *Science* 231, 999–1002 (1986).
27. Bowling, D. B. Light responses of ganglion cells in the retina of the turtle. *J. Physiol. (Lond.)* 299, 173–196 (1980).
28. Rosenberg, A. F. & Ariel, M. Electrophysiological evidence for a direct projection of direction-sensitive retinal ganglion cells to the turtle's accessory optic system. *J. Neurophysiol.* 65, 1022–1033 (1991).
29. Berry, M. J., Warland, D. K. & Meister, M. The structure and precision of retinal spike trains. *Proc. Natl Acad. Sci. USA* 94, 5411–5416 (1997).
30. Keat, J., Reinagel, P., Reid, R. C. & Meister, M. Predicting every spike: a model for the responses of visual neurons. *Neuron* 30, 803–817 (2001).
31. Stanley, G. B., Li, F. F. & Dan, Y. Reconstruction of natural scenes from ensemble responses in the lateral geniculate nucleus. *J. Neurosci.* 19, 8036–8042 (1999).
32. Nothmore, D. P. M. & Granda, A. M. Ocular dimensions and schematic eyes of freshwater and sea turtles. *Vis. Neurosci.* 7, 627–635 (1991).
33. Jones, K. E., Campbell, P. K. & Normann, R. A. A glass/silicon composite intracortical electrode array. *Ann. Biomed. Eng.* 20, 423–437 (1992).
34. Seung, H. S. & Sompolinsky, H. Simple models for reading neuronal population codes. *Proc. Natl Acad. Sci. USA* 90, 10749–10753 (1993).
35. Rujan, P. A fast method for calculating the perceptron with maximal stability. *J. Phys. (Paris)* 3, 277–290 (1993).